

MOLECULAR DYNAMICS STUDIES OF THE INTERACTION BETWEEN WATER AND OXIDE SURFACES

E. Dushanov^{a,b}, *Kh. Kholmurodov*^{a,c}, *K. Yasuoka*^d

^a Joint Institute for Nuclear Research, Dubna

^b Institute of Nuclear Physics, Ulugbek, Tashkent

^c «Dubna» International University for Nature, Society, and Man, Dubna, Russia

^d Department of Mechanical Engineering, Keio University, Yokohama, Japan

The water–surface interaction is a research target of great importance for a broad spectrum of technological applications and fundamental scientific disciplines. In the present study, a comparative analysis is performed to clarify the structural and diffusion properties of water on a number of oxide surfaces. Based on the molecular dynamics (MD) simulation method, the water–surface interaction mechanism was investigated for the oxide materials TiO₂ (anatase), Al₂O₃ (corundum), and Fe₂O₃ (hematite). A comparison of the water–TiO₂ interaction with the water–Al₂O₃ and water–Fe₂O₃ systems demonstrates the specificity of the adsorption and layer formation on the atomic/molecular level scale. The obtained MD analysis data point to a considerable enhancement of water–TiO₂ surface adsorption and a relatively high density distribution profile near the surface. The novel data on water structure and diffusion on oxide surfaces are discussed from the point of view of possible material innovation and design.

Взаимодействие воды с поверхностью является одной из наиболее важных задач для широкого спектра технологических приложений и с точки зрения фундаментальных научных дисциплин. В настоящей работе проведен сравнительный анализ структурных и диффузионных свойств воды на поверхности оксидных материалов. Особенности взаимодействия воды с поверхностью были исследованы с помощью метода молекулярной динамики (МД) для TiO₂ (анатаз), Al₂O₃ (корунд) и Fe₂O₃ (гематит). Особенности взаимодействия в системах вода–TiO₂, вода–Al₂O₃ и вода–Fe₂O₃ демонстрируют существенное различие в протекании адсорбционных процессов и формировании регулярных слоистых образований на атомарно-молекулярном уровне. Сравнительный анализ процессов при взаимодействии вода–поверхность указывает на значительную адсорбционную способность поверхности TiO₂, а также на более плотное распределение молекул воды вблизи нее. Обсуждается возможность применения полученных МД-данных при создании новых оксидных материалов с участием водных и других жидких соединений.

PACS: 83.10.Rs; 31.15.xv; 87.10.Tf; 87.15.ap; 47.11.Mn; 61.20.Ja; 61.43.Bn

INTRODUCTION

The interaction of water with surfaces is a topic of great interest in both material and life sciences taking into account a surprisingly broad technological application of the phenomena. Understanding the water–surface interaction mechanism is critically important for chemical and pharmaceutical industries, as well as for the fabrication of new materials and drugs [1–3].

The water–surface interaction is also a long-studied subject in a wide variety of fundamental scientific disciplines [4].

The oxide surface is a special target of research, and the interaction mechanism between water and oxide materials has been a subject of intense study in recent years. In this regard, one has to mention the following three oxide materials: TiO_2 (anatase), Al_2O_3 (corundum), and Fe_2O_3 (hematite). In surface chemistry, much of research on water–titanium oxides (TiO_2 's) has been motivated by the relatively high efficiency of TiO_2 in the photocatalytic decomposition of water. The water– TiO_2 interaction is potentially important as a solar energy conversion process. The photocatalytic properties of these materials in aqueous media have been studied since the mid-1970s [1]. These studies have inspired, in particular, work on well-characterized single crystals of oxides.

Titanium dioxide (TiO_2 , anatase) surfaces have been of the most interest concerning the photochemical degradation of organic compounds such as bactericides and hydrophobic coatings [2]. The TiO_2 –water reactions show a considerable potential in the field of solar energy conversion by means of the photocatalytic splitting of water (the Fujishima–Honda reaction in [3]).

Aluminum oxide (Al_2O_3 , corundum) has attracted particular interest due to its widespread use as catalyst and catalyst support. On these surfaces, exposure of dehydroxylated alumina to water vapor leads partly to rehydroxylation (for sample temperatures above 320 K) and partly to coordination of water molecules to exposed aluminum ions [5]. Water can be adsorbed in multilayer states by hydrogen bonding to the first-layer OH or H_2O groups, under favorable conditions of temperature and pressure.

Adsorption of water on iron oxide (Fe_2O_3 , hematite) surfaces is important in the oxidative corrosion and passivation of steels [6,7]. Doped iron oxides are also promising materials for the production of electrochemical solar energy conversion cells which split H_2O (e.g., [8–11]). Similarly, Kurtz and Henrich use UPS to show that H_2O is adsorbed dissociatively on an α - Fe_2O_3 (hematite) surface at room temperature, with dissociation occurring more readily (at a lower exposure) on a surface with a high defect density than on an annealed surface [12].

To the best of our knowledge, little literature or experimental data is available on the water– TiO_2 , water– Al_2O_3 , and water– Fe_2O_3 interaction mechanism on the atomic or molecular level. In the present paper, using the MD simulation method, we perform a comparative analysis of the water–surface interaction process for these oxide materials. We aimed at analyzing the structural and diffusion properties of water on oxide surfaces at similar simulation and thermodynamical conditions.

1. METHOD

A classical molecular dynamics study was performed using the DL_POLY_2.19 [13] general-purpose code. The NVT ensemble at $T = 300$ K in conjunction with a Nosé–Hoover thermostat with the direct Coulombic summation and the Verlet leapfrog scheme were employed. The integration time step of the dynamical equations of motion was 1 fs. All simulations were periodic in three dimensions.

For the oxide surfaces, the force fields as reported by Kavathekar et al. [14] and Guillot et al. [15] were used. For the TiO_2 surface, the potential parameters were developed by Matsui and Akaogi [16]. For the Al_2O_3 and Fe_2O_3 surfaces, the potential parameters were

developed by Guillot and Sator [15]. The Van der Waals (VdW) interaction between water and oxide surfaces was represented by the Lennard–Jones (lj) potential. The cross-interaction parameters for oxide surfaces and water models are summarized in Tables 1 and 2. The water bond angles and lengths were not constrained; thus, an SPC rigid body model was used. A parallel Shake algorithm expressed in terms of the Replicated Data strategy for constraining the rigid and other chemical bonds was used [13]. The MD simulations were realized at moderate temperatures of 250–375 K with a step of 25 K. For each simulation set, the MD calculations were ranged between 50,000–100,000 time steps of the integration of the equations of motion.

The LJ potential parameter in Table 2 for the Ti–OW pair seems to be large: $\varepsilon_{ij} = 7.72528$ kcal/mol — compared with others. Such a large ε_{ij} value for the Ti–OW pair was pointed out in other studies, too (see, for example, [17]). Nevertheless, our MD calculation results (as described below) exhibit a less or no dependence on the VdW interaction parameters of Table 2. For example, performing the test calculations with the following several values: $\varepsilon_{ij} = 7.72528$; $7.72528/10$; $7.72528/100$ kcal/mol — we got similar results. All the VdW

Table 1. The parameters of the Buckingham potential for TiO₂, Al₂O₃, Fe₂O₃: $A_{ij} \exp(-r_{ij}/\rho_{ij}) - C_{ij}/r_{ij}^6$

$l-j$	A_{ij} , kcal·mol ⁻¹	ρ , Å	C_{ij} , kcal·mol ⁻¹ Å ⁶
Ti–Ti	717647.4	0.154	121.067
Ti–OTi	391049.1	0.194	290.331
OTi–OTi	271716.3	0.234	696.888
Al–Al	658112.9	0.219	1379.831
Al–OAl	433092.1	0.172	797.385
OAl–OAl	208071.2	0.265	1962.278
Fe–Fe	184952.2	0.228	981.139
Fe–OFe	196511.7	0.190	0.0
OFe–OFe	208071.2	0.265	1962.278

Table 2. The parameters of the Lennard–Jones potential for TiO₂, Al₂O₃, Fe₂O₃ and water: $q_i q_j / r_{ij} + \varepsilon_{ij} [(\sigma_{ij}/r_{ij})^{12} - (\sigma_{ij}/r_{ij})^6]$

$l-j$	ε_{ij} , kcal·mol ⁻¹	σ_{ij} , Å
Ti–OW	7.72528	2.3431
Al–OW	0.11000	3.5000
Fe–OW	0.05350	3.6500
OTi–OW	0.22784	3.1306
OAl–OW	0.15543	3.5532
OFe–OW	0.15543	3.5532
OW–OW	0.15543	3.5532

Note. Atomic charges:
 $q(\text{Ti}) = 2.196e$, $q(\text{OTi}) = -1.098e$;
 $q(\text{Al}) = q(\text{Fe}) = 1.418e$, $q(\text{OAl}) = q(\text{OFe}) = -0.945e$;
 $q(\text{OW}) = -0.82e$, $q(\text{HW}) = 0.41e$.

interaction parameters shown in Tables 1 and 2 were slightly varied in their reasonable ranges; however, the final results do not exhibit any substantial difference here. Also, the results that we obtained using potentials other than the LJ (e.g., the Buckingham potential) for the water–oxide surface interaction were close to each other.

For each oxide surface, we have simulated various water densities (from low- to high-density phases) in the range of $\rho = 0.1\text{--}1.0$ g/cm³. The MD simulation results of the water–surface interaction which are summarized below are shown for: (1) $\rho = 0.3$ g/cm³ (343 water molecules), (2) $\rho = 0.5$ g/cm³ (512 water molecules), and (3) $\rho = 0.8$ g/cm³ (729 water molecules).

The bulk TiO₂ is defined by the lattice vectors of the following length: $a_0 = b_0 = 3.785$ Å, $c_0 = 9.514$ Å, bulk Al₂O₃ — by $a_0 = b_0 = 4.754$ Å, $c_0 = 12.990$ Å, and bulk Fe₂O₃ — by $a_0 = b_0 = 5.038$ Å, $c_0 = 13.772$ Å, respectively.

For the TiO₂ surface, we have simulated 192 molecules (2304 atoms); for the Al₂O₃ surface — 98 molecules (2940 atoms); and for Fe₂O₃ — 72 molecules (2160 atoms).

Table 3. The geometry details and molecular composition of the simulated water–oxide surface models

Surface	X, Å	Y, Å	Z, Å	System size
TiO ₂	30.280	30.280	61.203	(TiO ₂) ₂₃₀₄ (H ₂ O) ₁₀₂₉
Al ₂ O ₃	33.278	33.278	58.641	(Al ₂ O ₃) ₂₉₄₀ (H ₂ O) ₁₀₂₉
Fe ₂ O ₃	30.228	30.228	60.205	(Fe ₂ O ₃) ₂₁₆₀ (H ₂ O) ₁₀₂₉

The corresponding system sizes and molecular composition for $\rho = 0.3$ g/cm³ are specified in Table 3.

2. RESULTS AND DISCUSSIONS

2.1. Oxide Surfaces. First, we have investigated the structural peculiarities of the oxides TiO₂, Al₂O₃, and Fe₂O₃ based on their radial distribution functions (RDFs). The surface temperature variations in the interval of 250–375 K had no visible effect because here the structure of the oxide materials was stable. In Figs. 1, RDFs $g(r)$ are calculated for the final relaxed states of the oxide surfaces as follows: (top) anatase–anatase, (middle) corundum–corundum, and (bottom) hematite–hematite.

The RDFs are presented for the following atomic pairs: Ti–Ti and Ti–O; Al–Al and Al–O; Fe–Fe and Fe–O (top left and right; middle left and right; and bottom left and right, respectively).

From Figs. 1 we see that the Ti–Ti and Ti–O interactions (top left and right) are much stronger because here the RDF amplitudes are large. In other words, the RDFs of the atomic pairs of the TiO₂ material are much more ordered with respect to the Al₂O₃ and Fe₂O₃ systems. The RDFs of the Ti–Ti and Ti–O atomic pairs have sharp and separate peaks; for the Al–Al, Al–O (middle: left and right), Fe–Fe, and Fe–O (bottom: left and right) atomic pairs, the RDF peaks look relatively smoother. Thus, comparing the structural RDF data, we have clearly a more ordered TiO₂ system (top: left and right). For the atomic pairs Ti–O, Al–O, and Fe–O with the opposite charges, we observe their strong interactions; such behavior agrees with the results reported in literature earlier [18–20].

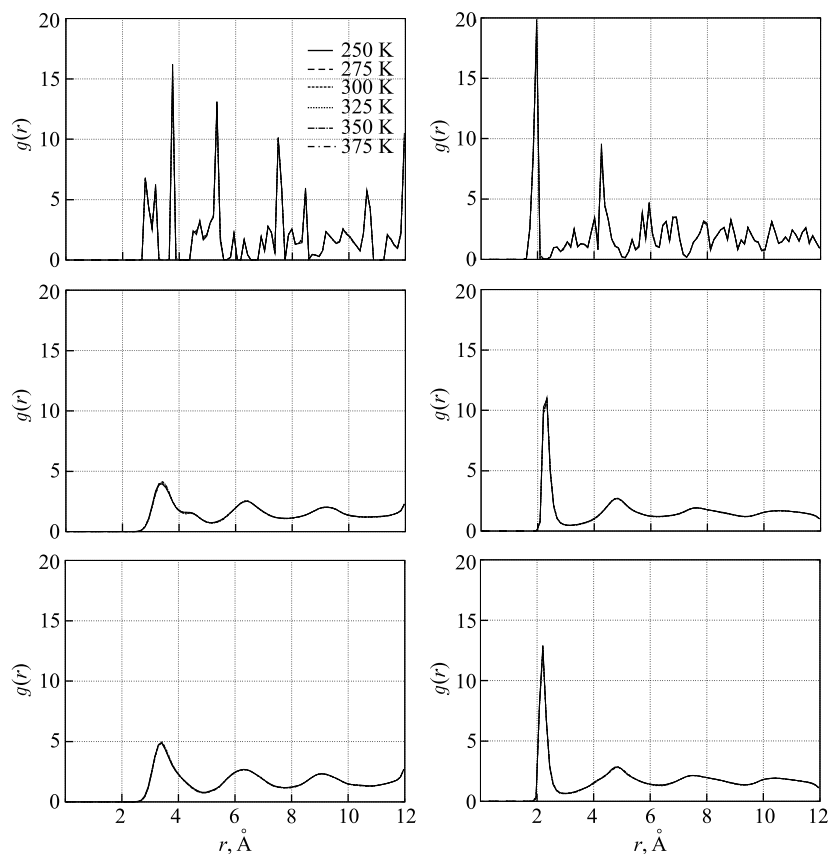


Fig. 1. The radial distribution functions (RDFs) of the surface–surface atomic pair interactions. Top: titanium–titanium (Ti–Ti) and titanium–oxygen (Ti–O_{Ti}); middle: aluminum–aluminum (Al–Al) and aluminum–oxygen (Al–O_{Al}); bottom: iron–iron (Fe–Fe) and iron–oxygen (Fe–O_{Fe}) (left and right, respectively)

2.2. Oxide Surfaces–Water Interactions. Figures 2 and 3 demonstrate the RDFs of the surface–water interactions at three water densities mentioned above: anatase–water (top), corundum–water (middle), and hematite–water (bottom).

In Figs. 2, the RDF behavior is presented for the following atomic pairs: Ti–OW, Al–OW, and Fe–OW (top, middle, and bottom, respectively).

From Figs. 2 (top) it is seen that the Ti–OW atomic pair RDF has large amplitudes characterizing the strong interatomic bonding of these atoms. The first RDF peak value of the Ti–OW pair is around 2, which is an order of magnitude higher than that of the Al–OW and Fe–OW ones. For the Ti–OW pair, the first RDF peak is seen at $r \sim 2 \text{ \AA}$, indicating a close-contact water–surface bonding; for the Al–OW and Fe–OW pairs (middle and bottom, left), the first RDF peak is located at $r \sim 3 \text{ \AA}$.

The next water layer (that is, the second RDF peak) for the Ti–OW pair can be seen at $r \sim 4 \text{ \AA}$ with zero between the first and second peaks. For the Al–OW and Fe–OW pairs, the

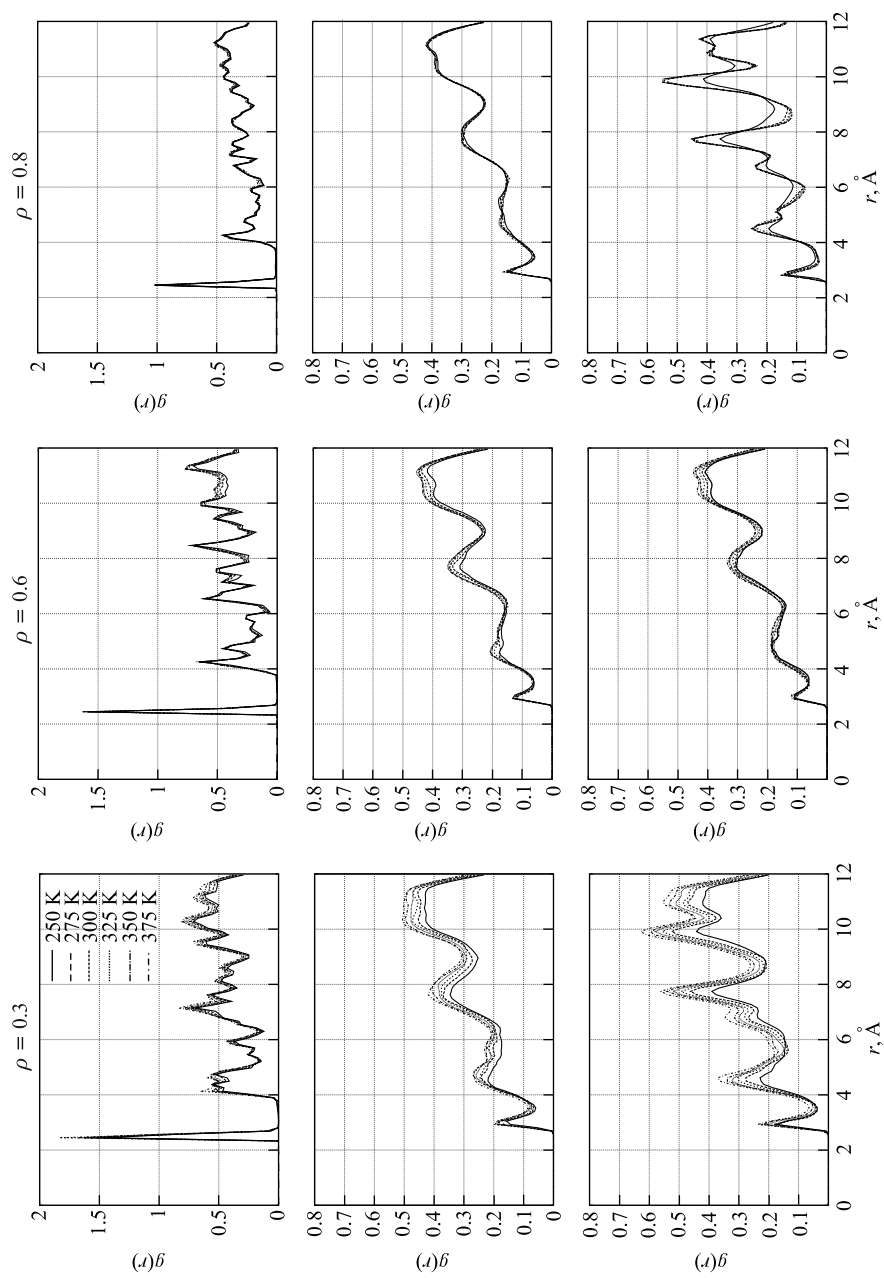


Fig. 2. The radial distribution functions (RDFs) of the surface-water atomic pair interactions (top: anatase-water (Ti-OW); middle: corundum-water (Al-OW); bottom: hematite-water (Fe-OW)) at three water densities

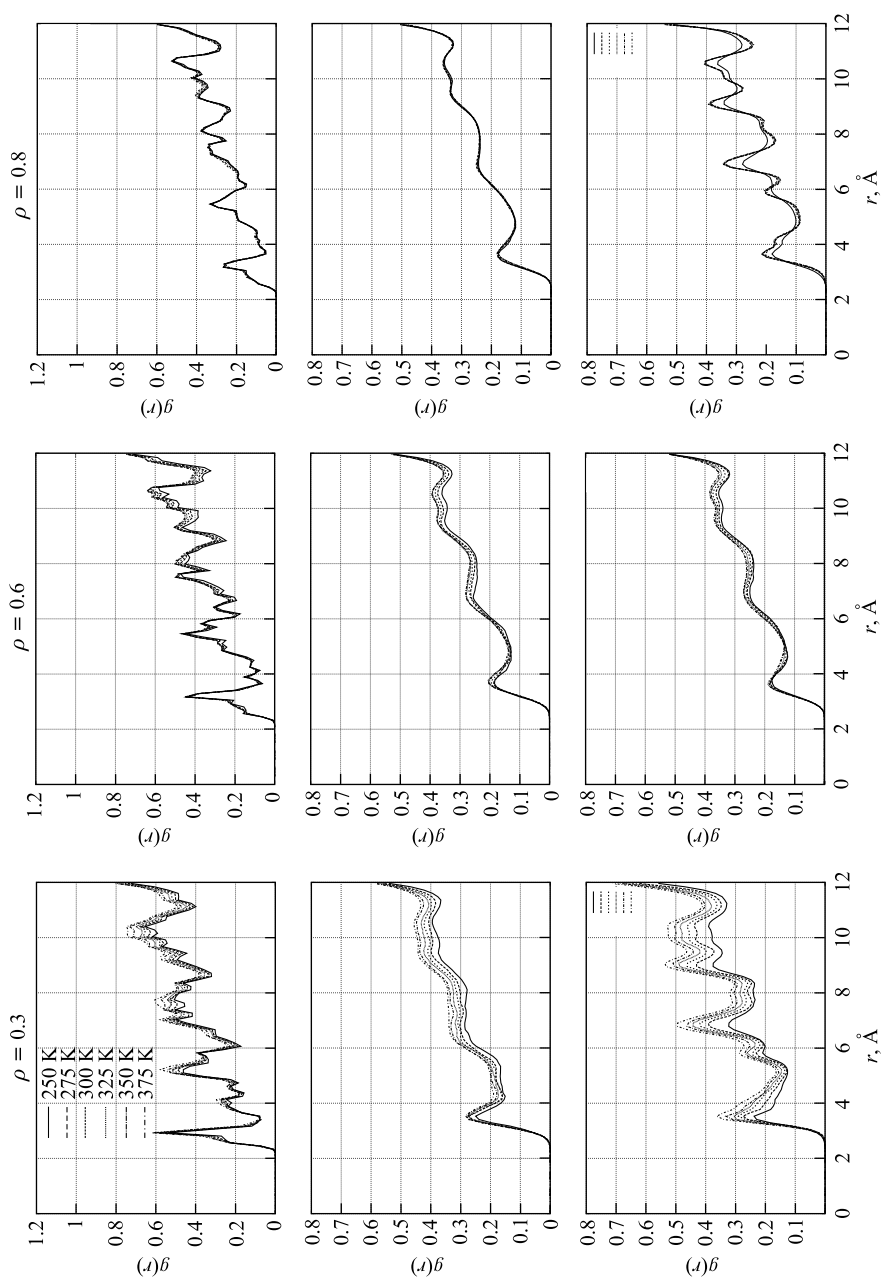


Fig. 3. The radial distribution functions (RDFs) of the surface-water atomic pair interactions (top: anatase-water (Ti-HW); middle: corundum-water (Al-HW); bottom: hematite-water (Fe-HW)) at three water densities

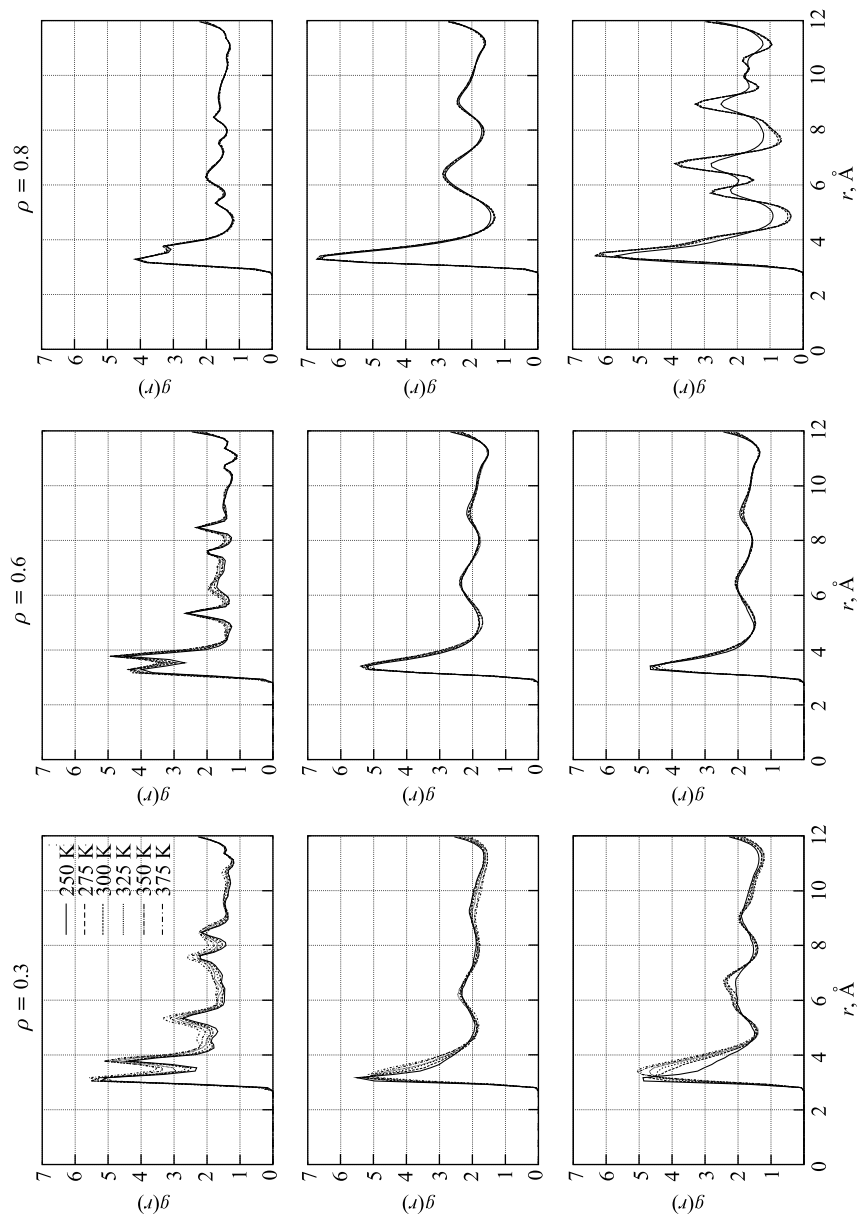


Fig. 4. The radial distribution functions (RDFs) of the water–water atomic pair interactions on oxide surfaces (top, left to right: OW–OW on anatase (TiO₂); middle, left to right: OW–OW on corundum (Al₂O₃); bottom, left to right: OW–OW on hematite (Fe₂O₃)) at three water densities.

second RDF peak is observed at $r \sim 5$ Å; the RDF distributions between the first and second peaks are nonzero unlike those of the Ti–OW ones.

In Figs. 3, RDF graphs are shown for the Ti–HW (top), Al–HW (middle), and Fe–HW (bottom) atomic pairs at three water densities, respectively.

The Ti–HW pair RDF (top) becomes weaker than that of the Ti–OW pair above. For the Al–HW and Fe–HW (middle and bottom) pairs, the structural RDF has a slightly larger first peak.

For the water–surface interactions, the structural RDFs correlate with surface peculiarities. A comparison of Figs. 2 and 3 with Figs. 1 is straightforward.

2.3. Water–Water Interactions. Next, we analyse the water–water interaction influenced by the presence of oxide surfaces at three water densities. Figures 4 and 5 represent water–water structural RDFs for the surfaces TiO₂ (top), Al₂O₃ (middle), and Fe₂O₃ (bottom). In Figs. 4 and 5, the RDFs are shown for the oxygen–oxygen (OW–OW) and hydrogen–hydrogen (HW–HW) atomic pairs, respectively.

From Figs. 4 it is seen that in the presence of the TiO₂ surface, the first RDF peak of the OW–OW pair splits slightly into two ones at 3–4 Å. Further, with increasing the water density, the first RDF peak of TiO₂ is modified (top, from left to right); thus, we can observe another two or three small but clear RDF peaks at $r = 5$ and 7–8 Å.

The first RDF peaks of Al₂O₃ (middle, from left to right) and Fe₂O₃ (bottom, from left to right) look rather broad in comparison with the one of OW–OW of TiO₂. The secondary OW–OW RDF peaks for the Al₂O₃ and Fe₂O₃ systems are weaker and located further than the TiO₂ one.

In Figs. 5, the RDF of the HW–HW pair of the TiO₂ system (top, from left to right) has two clear peaks at 2–4 Å in the case of a low water density. For the Al₂O₃ and Fe₂O₃ systems (middle and bottom, from left to right), the first RDF peaks for HW–HW are quite negligible. Thus, considering the water–water structural RDFs, we conclude that the structure formation here is mostly determined by the presence of the anatase surface. The water–water interaction is strongly influenced by the TiO₂ surface, which modifies the $g(r)$ behavior in comparison with that of Al₂O₃ and Fe₂O₃ ones.

2.4. Configuration Snapshots and Density Distribution Profiles. In Figs. 6, 3D configuration snapshots are displayed in the low water density case for the water–anatase (top), water–corundum (middle), and water–hematite (bottom) systems. The left and right snapshots correspond, respectively, to the initial and final relaxed states of the dynamics of water interaction with the oxide surfaces.

At a low density, water adsorption clearly dominates over the diffusion process and is more effective on the anatase (TiO₂) surface. Compared to the TiO₂ oxide surface, the other two ones, Al₂O₃ and Fe₂O₃, exhibit relatively weak adsorption capabilities. The TiO₂ surface structure remains well-ordered during all the dynamical changes. In contrast with TiO₂, the volume and surface oscillations of the Al₂O₃ and Fe₂O₃ oxides are notably larger. Although all the dynamical interaction processes take place around room temperature, Al₂O₃ and Fe₂O₃ undergo significant modifications and behave like amorphous materials. Hence, the oxide structure variations affect the water density distribution near the surfaces.

In Figs. 7, plots of the density of water molecules as a function of the perpendicular distance from the surface are presented for TiO₂ (top), Al₂O₃ (middle), and Fe₂O₃ (bottom), respectively, for three water densities. All the water Z -density profiles in Figs. 7 are normalized to the bulk solution density.

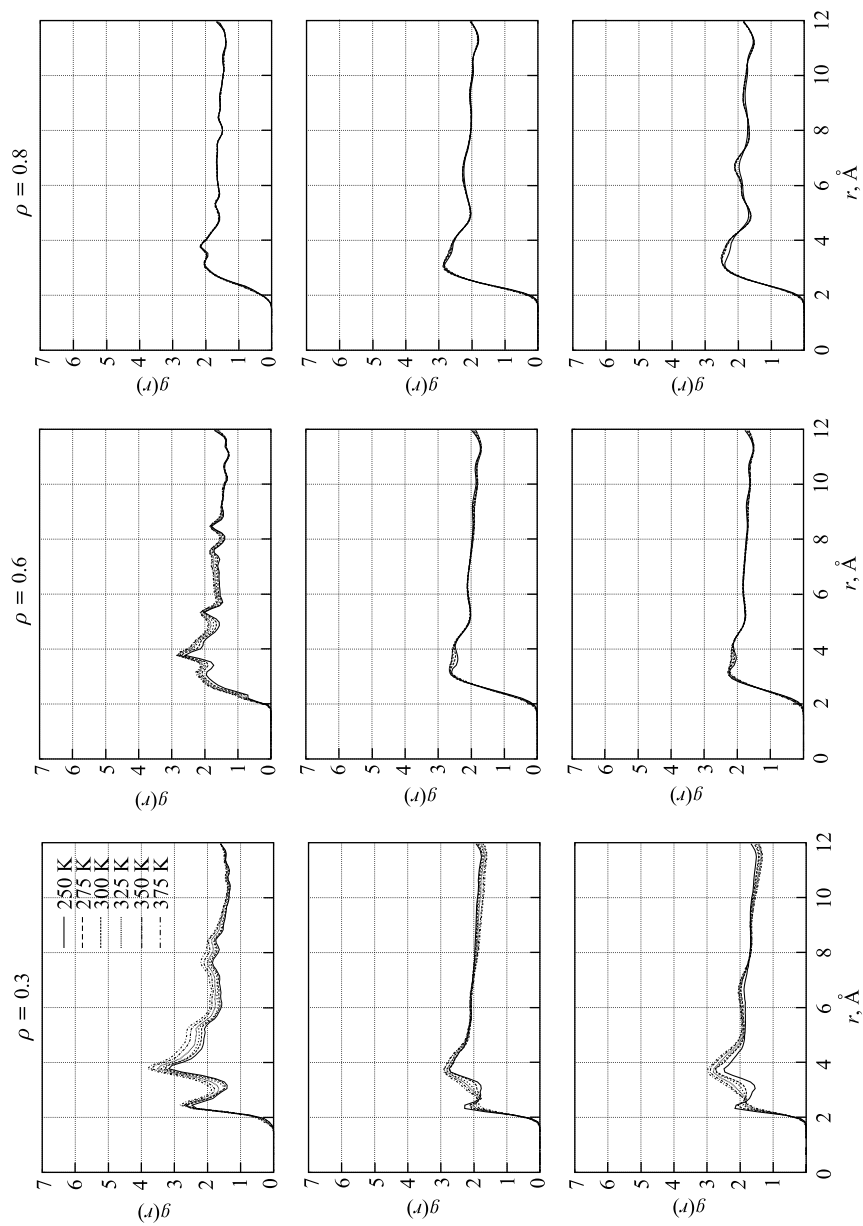


Fig. 5. The radial distribution functions (RDFs) of the water–water atomic pair interactions on oxide surfaces (top, left to right: HW–HW on anatase (TiO₂); middle, left to right: HW–HW on corundum (Al₂O₃); bottom, left to right: HW–HW on hematite (Fe₂O₃)) at three water densities

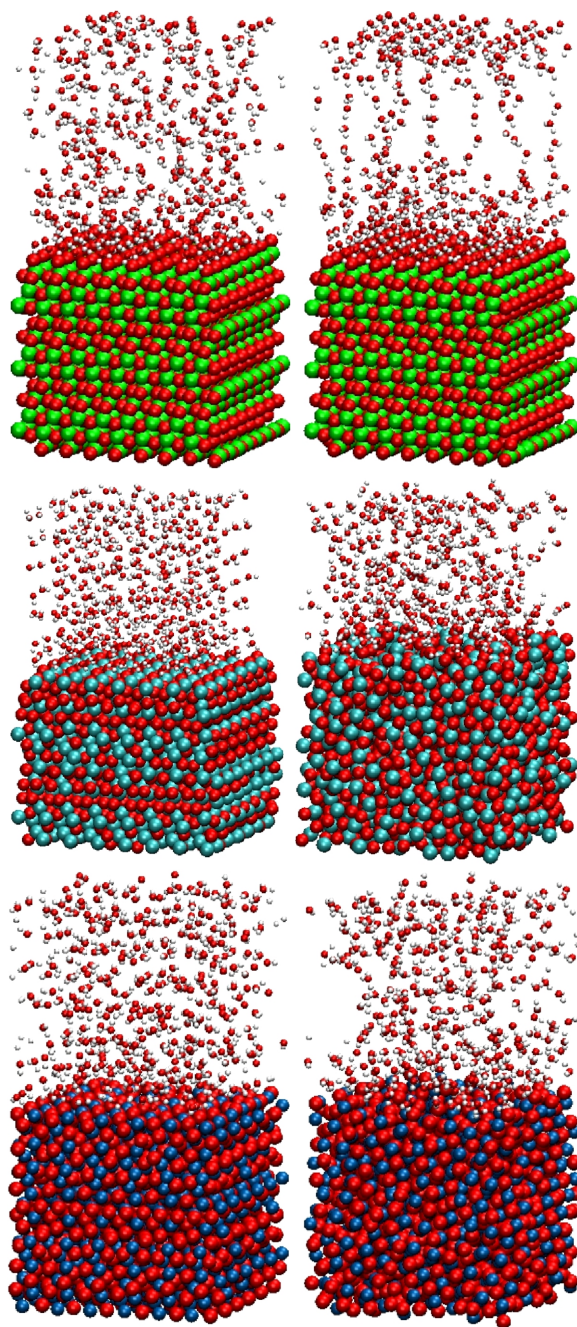


Fig. 6. Configuration snapshots of water on oxide surfaces in the initial (left) and final relaxed (right) states (top: water–anatase ($\text{H}_2\text{O}-\text{TiO}_2$); middle: water–corundum ($\text{H}_2\text{O}-\text{Al}_2\text{O}_3$); bottom: water–hematite ($\text{H}_2\text{O}-\text{Fe}_2\text{O}_3$))

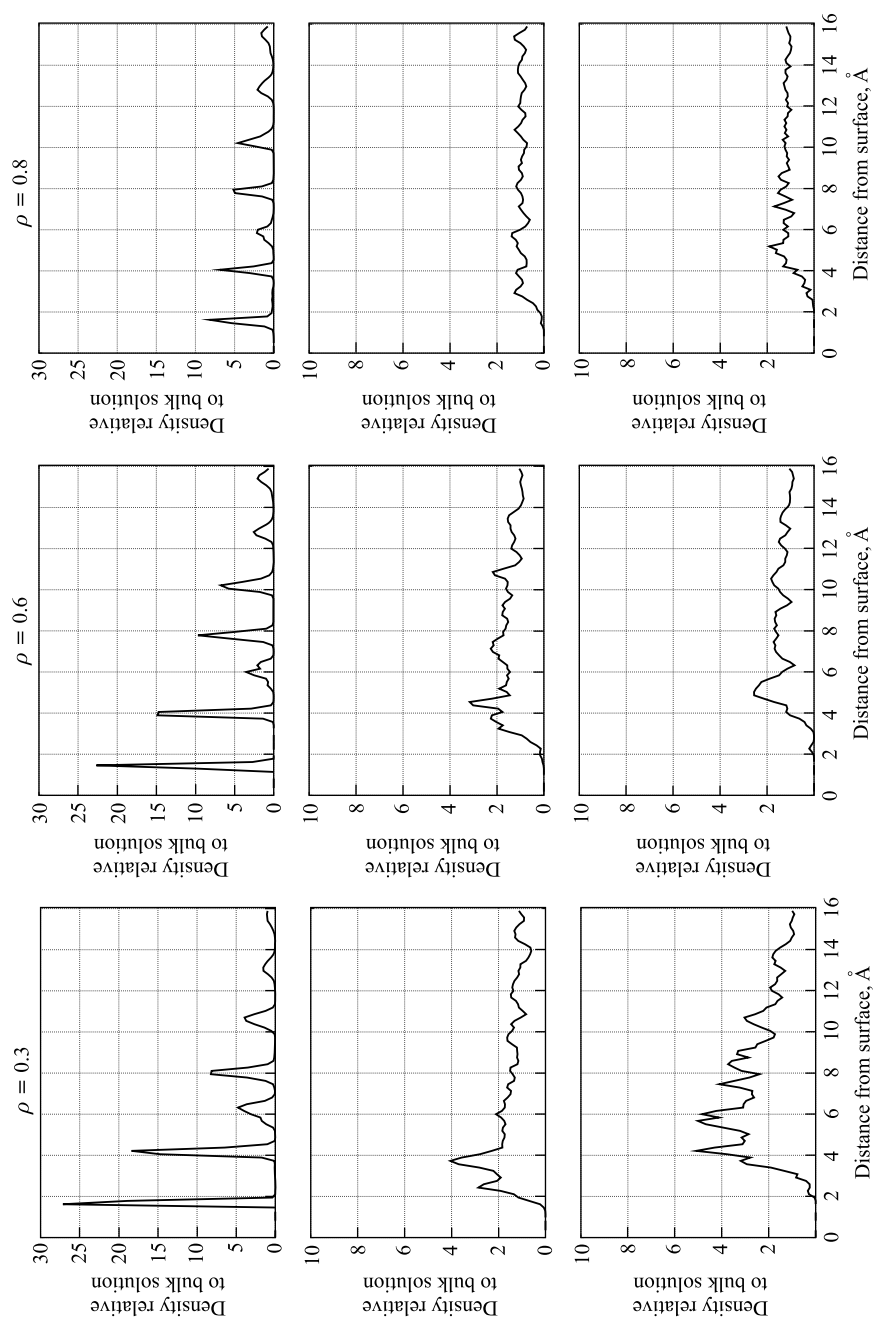


Fig. 7. Z-density profiles of water on oxide surfaces (top: water-corundum ($\text{H}_2\text{O}-\text{Al}_2\text{O}_3$); middle: water-anatase ($\text{H}_2\text{O}-\text{TiO}_2$); bottom: water-hematite ($\text{H}_2\text{O}-\text{Fe}_2\text{O}_3$))

Figures 7 (top, left to right) show that the water–TiO₂ system has well-defined adsorption layers, formed as a result of the presence of an oxide surface. The Z -density amplitudes of these adsorption layers correlate with the water densities up to the dense water phases.

The results of Figs. 7 show that the density of water molecules on the anatase surface is several orders of magnitude higher than on other surfaces. The water density distribution on the TiO₂ surface relative to the bulk density is considerably higher and well-layered. For example, for low water densities, the first water layer on the anatase surface is about 28 units; while on the corundum and hematite surfaces, about 2.5–3 units. The second layer on the anatase surface is about 18 units; on corundum, it is about 4; and on hematite, about 5 units. The adsorbance properties of surfaces change zigzag-like with the distance between water molecules and the corresponding surface. This distance is 1.2 Å for anatase; 1.1 Å for corundum; and 1.8 Å for hematite.

2.5. Diffusion Coefficients. At three water densities, data on the diffusion coefficient $D(T)$ for bulk water are presented for all oxide surfaces in Figs. 8. For the TiO₂ surface (left and middle) at low water densities, strong water adsorption takes place and it dominates over the diffusional mobility of the water molecules. For the water–Al₂O₃ and water–Fe₂O₃ systems, the $D(T)$ law is quite similar.

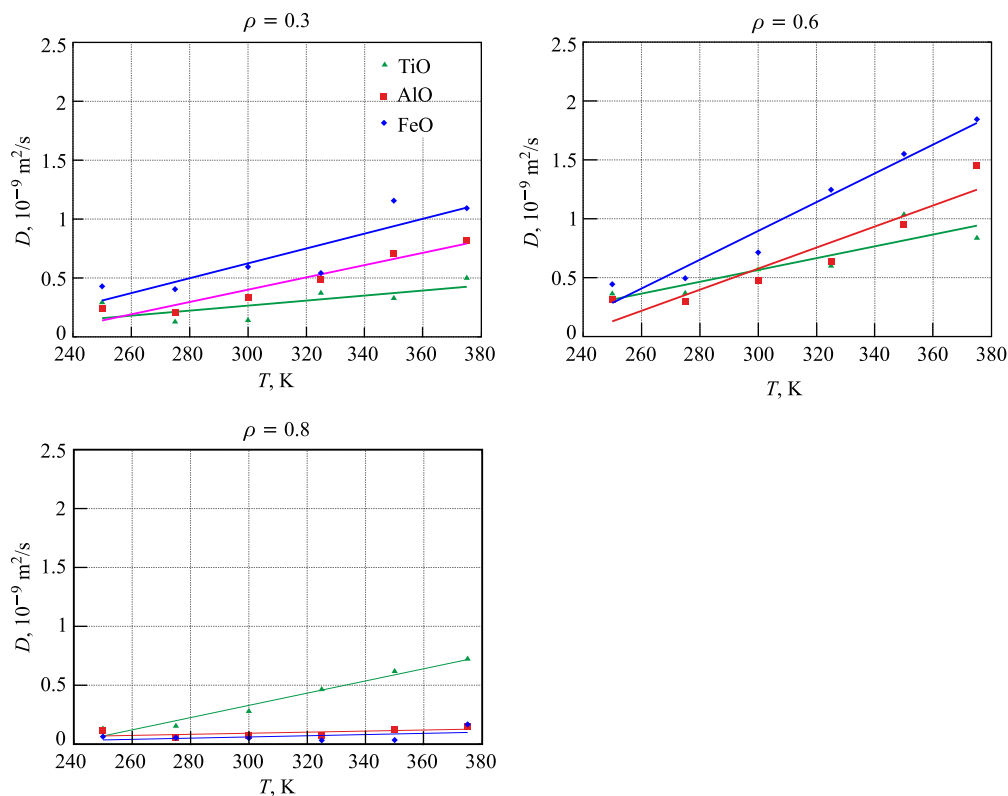


Fig. 8. (Color on-line) The temperature dependence of the diffusion coefficient of water on the oxide surfaces (green: water–anatase (H₂O–TiO₂); pink: water–corundum (H₂O–Al₂O₃); blue: water–hematite (H₂O–Fe₂O₃))

With increasing the water density, strong water–TiO₂ interaction results in a greater diffusion coefficient than the one for the water–Al₂O₃ and water–Fe₂O₃ systems. The diffusional mobility of water molecules becomes relatively large for the TiO₂ surface (right).

The diffusion coefficient $D(T)$ behavior is in good agreement with the structural RDFs and Z -density profiles described above. The TiO₂ surface reveals an extreme adsorption ability, so here we have a considerable enhancement of bulk water adsorption. Strong water adsorption, together with the well-structured TiO₂ surface, results in the presence of well-defined layered water formations.

CONCLUSION

Using the molecular dynamics simulation method for three oxide systems (TiO₂, Al₂O₃ and Fe₂O₃), the structural, dynamical, and diffusion properties of water have been analyzed in its low- and high-density phases. First, the peculiarities of the oxide structures have been investigated, and the structural data have been found to be in good agreement with previously reported results in the literature. For the water–oxide surfaces, the RDF of the Ti–OW atomic pair interactions has the largest amplitude characterizing the strong interatomic bonding of these atoms. The first RDF peak for the Ti–OW pair is around 2, which is an order of magnitude higher than the one of the Al–OW and Fe–OW pairs (0.2). For water–water interaction, we observe enhanced structure formation influenced by the anatase (TiO₂) surface, which is expressed in the RDF $g(r)$ behavior. In the presence of the TiO₂ surface, the first peak of the RDF of the OW–OW pair splits slightly into two ones at 3–4 Å; another two or three smaller but clear RDF peaks are observed at $r = 5$ and 7–8 Å. For the HW–HW pair, the RDF of the water–TiO₂ system has two clear peaks at 2–4 Å, while for the Al₂O₃ and Fe₂O₃ systems, the first RDF peaks of the HW–HW system are quite negligible. The plot of the density of water molecules was built as a function of the perpendicular distance from the surface and compared for the TiO₂, Al₂O₃, and Fe₂O₃ surfaces. For the water–TiO₂ system, the density profile plot reveals the formation of well-defined adsorption layers. The water density on the TiO₂ surface is relatively large: several orders of magnitude higher than on other oxide surfaces. The diffusion coefficients of the bulk water $D(T)$ have been calculated and compared for all oxide surfaces. The $D(T)$ diffusion coefficient law has been found to be in good agreement with the structural RDFs and Z -density profiles near the oxide surfaces. At low water densities, strong adsorption on the TiO₂ surface dominates over the diffusional mobility of the water molecules. At high water densities, the TiO₂ surface has an extreme adsorption ability; so, we observed a considerable enhancement of water diffusion in a bulk solution.

With a view to the possible modification and design of oxide materials, our MD simulation results agree well with several observations being widely discussed in today's literature and applied research. First, the paper [21] on noncrystal (liquid and amorphous) oxides should be mentioned. There is the issue of the affinity of the Fe₂O₃ and Al₂O₃ structures: peculiarities have been discussed that are similar to those in our observation reported above. An experimental investigation of the interaction of water and methanol with an anatase surface was performed in [22]. In particular, for water, three desorption states were observed in temperature-programmed desorption (TPD) spectra at 160, 190, and 250 K. The three desorption peaks were assigned to multilayer water, water adsorbed to 2-fold-coordinated O,

and water adsorbed to 5-fold-coordinated Ti, respectively. In [23] the studies report on hydroxylation and water adsorption on α -Fe₂O₃(0001) near the ambient conditions using ambient-pressure X-ray photoelectron spectroscopy (AP-XPS) that provides quantitative information on the in situ chemical composition of surfaces in equilibrium with water vapor in the Torr pressure range. The experiments were performed at pressures ($p(\text{H}_2\text{O}) \leq 2$ Torr) and temperatures ($T = 277$ – 647 K), covering a relative humidity range of up to 34%.

Acknowledgements. This work was performed in the framework of a collaboration between the Joint Institute for Nuclear Research (Dubna, Russia) and Keio University, Japan. This work was supported in part by the Grant in Aid for the Global Center of Excellence Program of the Center for Education and Research of Symbiotic, Safe and Secure System Design from the Ministry of Education, Culture, Sport, and Technology of Japan. The MD simulations have been performed using computing facilities, software, and clusters at JINR, Russia (CICC); RIKEN, Japan (RICC, MDGRAPE); and the Yasuoka Laboratory at Keio University, Japan. We thank Prof. Vladimir Korenkov (LIT, JINR) for providing us with computer time at CICC, and Prof. Evgeny Krasavin (LRB, JINR) for his encouraging support. The authors would like to especially thank Mr. Sergei Negovellov (JINR) for technical assistance and helpful comments.

REFERENCES

1. Hennch V. E. // Rep. Prog. Phys. 1985. V. 48. P. 1481; Prog. Surface Sci. 1979. V. 9. P. 143.
2. Diebold U. // Surface Sci. Rep. 2003. V. 48. P. 53.
3. Fujishima A., Honda K. // Nature. 1972. V. 238, No. 5358. P. 37.
4. Thiel P. A., Madey T. E. The Interaction of Water with Solid Surfaces: Fundamental Aspects // Surface Sci. Rep. 1987. V. 7. P. 211–385.
5. Knounger H. Hydrogen Bonds in Systems of Adsorbed Molecules // The Hydrogen Bond / Eds. P. Schuster, G. Zundel and C. Sandorfy. Amsterdam: North-Holland, 1976. V. 3, Ch. 27. P. 1263–1364.
6. Bartón K. Protection against Atmospheric Corrosion Theories and Methods. London; N. Y.: John Wiley and Sons Ltd., 1976.
7. Butler G., Ison H. C. K. Corrosion and Its Prevention in Waters. N. Y.: Reinhold Publ. Corp., 1966.
8. Sato S., White J. M. // Chem. Phys. Lett. 1980. V. 72. P. 83.
9. Leygraf C., Hendewerk M., Somorjai G. A. // J. Catalysis. 1982. V. 78. P. 341.
10. Turner J. E., Hendewerk M., Somorjai G. A. // Chem. Phys. Lett. 1984. V. 105. P. 581.
11. Leygraf C., Hendewerk M., Somorjai G. A. // J. Solid State Chem. 1982. V. 48. P. 35; J. Catalysis. 1982. V. 78. P. 341.
12. Kurtz R. L., Hennch V. E. // Phys. Rev. B. 1987. V. 36. P. 3414.
13. Smith W., Forester T. R., Todorov I. T. The DL_POLY User Manual / Ed. by Editor v. 2.20. 2009.
14. Kavathekar R. S. et al. Molecular Dynamics Study of Water in Contact with the TiO₂ Rutile-110, 100, 101, 001 and Anatase-101, 001 Surface // Mol. Phys. 2011. V. 109, No. 13. P. 1–8.
15. Guillot B., Sator N. A Computer Simulation Study of Natural Silicate Melts. Part I: Low Pressure Properties // Geochimica et Cosmochimica Acta. 2007. V. 71. P. 1249–1265.
16. Matsui M., Akaogi M. // Mol. Sim. 1991. V. 6. P. 239.

17. *Mitchell M. C., Gallo M., Nenoff T. M.* Computer Simulations of Adsorption and Diffusion for Binary Mixtures of Methane and Hydrogen in Titanosilicates // *J. Chem. Phys.* 2004. V. 121. P. 1910.
18. *Hoang V. V.* Molecular Dynamics Study on Structure and Properties of Liquid and Amorphous Al_2O_3 // *Phys. Rev. B.* 2004. V. 70. 134204.
19. *Khanh B. T. H. L., Hoang V. V., Zung H.* Structural Properties of Amorphous Fe_2O_3 Nanoparticles // *Eur. Phys. J. D.* 2008. V. 49. P. 325–332.
20. *Xiaobo Chen, Mao S. S.* Titanium Dioxide Nanomaterials: Synthesis, Properties, Modifications, and Applications // *Chem. Rev.* 2007. V. 107, No. 7. P. 2891–2959.
21. *Belashchenko D. K.* Computer Simulation of Structure and Properties of Non-crystalline Oxides // *Adv. Chem.* 1997. V. 66. P. 9 (in Russian).
22. *Herman G. S. et al.* Experimental Investigation of the Interaction of Water and Methanol with Anatase- $\text{TiO}_2(101)$ // *J. Phys. Chem. B.* 2003. V. 107. P. 2788–2795.
23. *Yamamoto S. et al.* Water Adsorption on $\alpha\text{-Fe}_2\text{O}_3(0001)$ at Near Ambient Conditions // *J. Phys. Chem. C.* 2010. V. 114, No. 5. P. 2256–2266.

Received on December 19, 2011.